Exploring the pseudo-ductility of aligned hybrid discontinuous composites using controlled fibre-type arrangements

J.M. Finley[a], H. Yu[b,c], M. L. Longana[b], S. Pimenta[a,*], M.S.P. Shaffer[d], K. D. Potter[b]

[a] *Department of Mechanical Engineering, South Kensington Campus, Imperial College London, SW7 2AZ, United Kingdom*
[b] *Bristol Composites Institute, Advanced Composites Collaboration for Innovation and Science, Queens Building, University Walk, Bristol, BS8 1TR, United Kingdom*
[c] *Department of Mechanical Engineering, University of Bath, Bath, BA2 7AY, United Kingdom*
[d] *Department of Chemistry, South Kensington Campus, Imperial College London, SW7 2AZ, United Kingdom*

Abstract

Pseudo-ductility presents a potential means for preventing catastrophic failure in composite materials; large deformations will prevent brittle fracture and provide warning before final failure. This work explores how the pseudo-ductility and strength of aligned hybrid discontinuous composites can be controlled by manipulating the arrangement of different fibre types. Aligned carbon/glass hybrid specimens with different fibre arrangements are manufactured and tested using a modification to the High Performance Discontinuous Fibre (HiPerDiF) method. Experimental results are complemented by an improved virtual testing framework, which accurately captures the fracture behaviour of a range of hybrid discontinuous composite microstructures. With a randomly *intermingled* fibre arrangement as a baseline, a 27% increase in strength and a 44% increase in pseudo-ductility can be achieved when low elongation fibres are completely *isolated* from one-another. Results demonstrate that the HiPerDiF method is the current state-of-the-art for maximising the degree of intermingling and hence the pseudo-ductility of hybrid composites.

Keywords: Pseudo-ductility, hybrid, microstructures, fracture,

1. Introduction

Composite materials are widely used in aerospace and automotive applications due to their high specific strength and specific stiffness [1]. However, composite materials often fail in a brittle manner, which may lead to catastrophic failure; consequently, composite structures are often over-designed and overweight. There is therefore a strong desire for

*Corresponding author.
Email address: soraia.pimenta@imperial.ac.uk (S. Pimenta)

Finley JM, Yu H, Longana ML, Pimenta S, Shaffer MSP, Potter KD (2018). Exploring the pseudo-ductility of aligned hybrid discontinuous composites using controlled fibre-type arrangements. *Composites Part A* 107, 592–606.DOI:10.1016/j.compositesa.2017.11.028

Nomenclature

General properties

n_*	number of (*)
v_f	fibre volume fraction
v_c	carbon ratio
ϕ	fibre diameter
w_*	width of (*)
t_*	thickness of (*)
ξ	RVE index
$\mathcal{G}_\mathrm{I}$	mode-I fracture toughness
$\mathcal{G}_\mathrm{II}$	mode-II fracture toughness
$\boldsymbol{T}$	matrix of fibre types
$\mathcal{U}$	random distribution sample
$\mathcal{N}$	normal distribution sample

Subscripts

f	fibre
c	carbon fibre
g	glass fibre
i	fibre row within specimen
j	fibre column within specimen
r	sub-region
RVE	representative volume element
s	specimen

Superscripts

k	cluster index
ε	strain increment

Manufacturing variables

ρ_A	areal density
ρ_f	fibre density
q	nozzle flow rate
b_f	fibre concentration in water
V	conveyor belt velocity

Migration variables

Δi	horizontal fibre migration
Δj	vertical fibre migration
ψ	migration fuzzy factor
σ_v	vertical migration std. dev.
σ_h	horizontal migration std. dev.
$\boldsymbol{\mu}_\mathrm{h}$	mean horizontal migration
m_h	horizontal migration factor
$\boldsymbol{D}$	matrix of fibre type changes

Stress, strain, and fracture variables

$\boldsymbol{\sigma}$	matrix of stresses
$\boldsymbol{\epsilon}$	matrix of strains
X_s	specimen ultimate strength
E_s	specimen initial stiffness
S_m	matrix shear strength
G_m	matrix shear modulus
A_f	unbroken fibre area ratio
$\boldsymbol{B}$	matrix of broken fibres
$\boldsymbol{C}$	matrix of clusters
$\boldsymbol{n}_\mathrm{k}$	no. clusters of broken fibres
$\boldsymbol{n}_{\mathrm{f_b}}$	no. fibres bordering a cluster
$\boldsymbol{a}_\mathrm{e}$	cluster equivalent crack sizes
$\boldsymbol{J}$	cluster strain energy release rates
$\boldsymbol{R}_\mathrm{min}$	matrix of min. reserve factors
$\boldsymbol{K}$	cluster position within the cross-section
$\boldsymbol{S}$	fibre positions surrounding a cluster

pseudo-ductile composites that fail more gradually and offer more warning before final failure [2].

One means of achieving pseudo-ductility in composite materials is through the use of aligned discontinuous reinforcements, which exploit the progressive failure of the matrix or fibre-matrix interface to promote gradual failure. The pseudo-ductility of aligned discontinuous composites was verified both analytically [3] and experimentally [4] at the ply-level, before being further demonstrated at the fibre-level using the HiPerDiF (High Performance Discontinuous Fibre) method to produce aligned discontinuous fibre compos-

ites [5].

Hybrid fibre composites can enhance pseudo-ductility via progressive fragmentation of low elongation fibres or plies and their subsequent partial debonding or delamination from the high-elongation material [6–8]. Yu et al. [9] modified the HiPerDiF method [5] to combine hybridisation with an aligned discontinuous microstructure to create an *intermingled* aligned hybrid discontinuous composite; this material contained well-aligned hybrid fibre types which are randomly placed within the cross-section of the specimen. The *intermingled* aligned hybrid discontinuous composite demonstrated pseudo-ductile strains of over 1%, both experimentally [9] and analytically [10].

Previous research suggests that the arrangement of hybrid fibre types has a significant influence on the structural performance of continuous fibre hybrid composites [11–14]. Most of the authors [11–13] reported that an increased dispersion of the hybrid fibre types (i.e. a highly *intermingled* fibre arrangement) increases the ultimate strain of the composite, although Swolfs et al. [14] argued that an *interlaminated thin-ply* arrangement leads to a larger hybrid effect on the apparent failure strain of the low-elongation fibres. However, similar studies have not been carried out for aligned hybrid *discontinuous* composite materials.

This paper aims to explore whether the arrangement of hybrid fibre types can influence the mechanical performance of aligned hybrid discontinuous composite materials. The scope of this work will cover both highly *intermingled* hybrid fibre arrangements, as well as microstructures with more grouped fibre-type arrangements (i.e. *intraply* [9] hybrids). Section 2 describes the techniques used to manufacture the specimens and to gather the experimental data. Section 3.1 describes a method that simulates the formation of the same type of microstructures that were created during the manufacture of the experimental specimens. An existing semi-analytical model [10] to predict the response of aligned hybrid discontinuous composites will be further improved in Section 3.2 with a new fracture toughness-based failure criterion, which is formulated specifically to analyse the fracture behaviour of both *intermingled* and *intraply* aligned hybrid discontinuous composite materials. Finally, results are shown and discussed in Section 4, and conclusions are drawn in Section 5.

2. Experimental development

2.1. HiPerDiF method for intraply aligned short fibre hybrid composites

The fibre orientation mechanism for the HiPerDiF method is described in previous work by Yu et al. [5, 9]. In summary, a suspension of fibres (dispersed in water) is supplied by nozzles to the fibre orientation head, which is composed of two thin-parallel plates that then align the fibres by a sudden momentum change, provided that the fibre length is less than the gap distance between the two parallel plates (see Figure 1).

A lab-scale prototype machine is capable of aligning discontinuous fibres, drying the remaining water on the fibres, and delivering the tape-type plies to the resin film impregnation stage, all in an in-line process. The desired ply width is achieved by placing a number of fibre orientation units next to each other (see Figure 1b), which results in a ply up to 5 mm wide. This process enables a high throughput, making it a strong candidate for industrialisation.

More importantly for this paper, the HiPerDiF method also allows for the manufacture of various types of hybrid discontinuous fibre arrangements. For instance, *intermingled* hybrid fibre arrangements can be easily manufactured if two or more types of fibres are dispersed in the water suspension [9]. Since the HiPerDiF method uses numerous nozzles, each one corresponding to a fibre orientation unit, *intraply* hybrids can also be generated, which feature a much lower level of intermingling, as shown in Figure 1. The HiPerDiF method was deemed the most suitable for this application as other manufacturing methods have limitations in controlling group (or bundle) size [15] and fibre dispersion [16] and are incapable of incorporating discontinuous reinforcements.

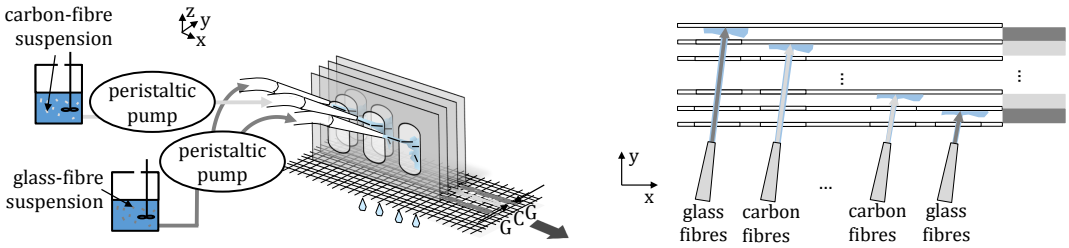

(a) *Intraply* hybrids are manufactured using separate nozzles and orientation heads, each supplying a suspension containing a single fibre type.

(b) The separate sub-regions combined to form a ply, which contains the different sub-regions across its width.

Figure 1: The HiPerDiF process, here shown in the modified version to produce *intraply* hybrid discontinuous composites with distinct carbon or glass subregions.

2.2. Materials and manufacturing condition

High modulus carbon (HMC, subscript 'c', represented in light grey in all figures) and E-glass (EG, subscript 'g', represented in dark grey in all figures) fibres were used in this paper; the properties of both fibre types are listed in Table 1. This fibre combination was selected because pitch-based high-modulus carbon fibres have a much lower failure strain than E-glass fibres, which promotes fibre fragmentation and increases the pseudo-ductility of the hybrid composite [9]. On the contrary, PAN-based discontinuous fibres feature a failure strain that is too similar to that of the E-glass fibres, and hence would not enable a pseudo-ductile response [9]. The HiPerDiF method enabled the manufacture of the *intermingled* and *intraply* hybrid intended cross sections shown in Figures 2a to 2e, with different intended HMC fibre group sizes and distributions, while keeping the intended carbon volume ratio in the composites at $v_c = 0.33$ (the carbon ratio (v_c) is defined such that $v_c + v_g = 1$).

Five intended cross-section fibre arrangements were manufactured; these are shown (not to scale) in Figures 2a to 2e. Each intended hybrid specimen is composed of four hybrid plies laid-up in the through-thickness direction, z. Each hybrid ply consists of a dry hybrid preform impregnated with an epoxy resin film (Cytec MTM49-3), the properties for which are shown in Table 1. The specimens are then laid-up in a mould, placed in a vacuum bag and then cured in an autoclave at 135°C for 135 minutes at 6 bar pressure.

Each *intraply* hybrid ply was manufactured using nine nozzles in parallel, with each nozzle connected individually to the HMC or EG suspension tanks, as shown in Figure 1a. Five unique *intraply* hybrid plies were manufactured, as shown in Figure 3a. A single stripe of a specific fibre type, which originates from a single nozzle (see Figure 3b), is hereby designated a sub-region (subscript 'r'). The plate spacing defines the width of each sub-region (w_r, set as 0.5 ±0.01 mm for 3 mm long fibres), while the areal density of each sub-region is defined by [17]:

$$\rho_{A_r} = \frac{q_r \cdot b_{f_r} \cdot \rho_{f_r}}{w_r \cdot V}, \tag{1}$$

where q_r is the flow rate per nozzle, b_{f_r} is the fibre concentration in the suspension (water), ρ_{f_r} is the fibre density, and V is the velocity of the conveyor belt.

The machine parameters were selected, as described in a previous paper [9], to obtain HMC and EG sub-regions with an areal density of 58 and 68 g/m^2 respectively. This allows the same overall fibre volume ($v_f = 0.3$) in each of the HMC and EG *intraply* hybrid composite cross sections. Figure 3c shows an example of *intraply* hybrid plies

Table 1: Material properties used for this paper. It should be noted that the fibre volume fraction (v_f) is set to 0.30 throughout this paper. Values with a † were estimated from work by Pardini and Manhani [18], while values with a ‡ were calculated using the method described by Henry and Pimenta [19].

Fibre-specific properties	High modulus carbon fibre	E-glass fibre
Fibre name	NGF XN90	Vectrotex C100
No. fibres in cross-section, n_f	1348	5474
Diameter, ϕ (μm)	10 [20]	7 [9]
Length, l (mm)	3 [9]	3 [9]
Young's modulus, E (GPa)	876 [20]	73 [9]
Weibull reference strength, X_f (MPa)	3460 [20]	2400 [9]
Weibull modulus, m	5 [20]	$5.65^\dagger$
Weibull gauge length, l_w (mm)	1 [20]	25 [9]
Composite fracture toughness, $\mathcal{G}_\mathrm{I}$ (kN/m^2)	$3.50^\ddagger$	$4.37^\ddagger$
Matrix / interface properties	MTM 49-3 epoxy	
Shear modulus, G_m (GPa)	1.5 [10]	
Interlaminar shear strength, X_m (MPa)	80 [21]	
Mode-II fracture toughness, $\mathcal{G}^\mathrm{c}_{\mathrm{II}_\mathrm{m}}$ (kJ/m^2)	0.8 [22]	
Pull-out frictional stress (SFPO), τ^0_μ (MPa)	10 [23, 24]	

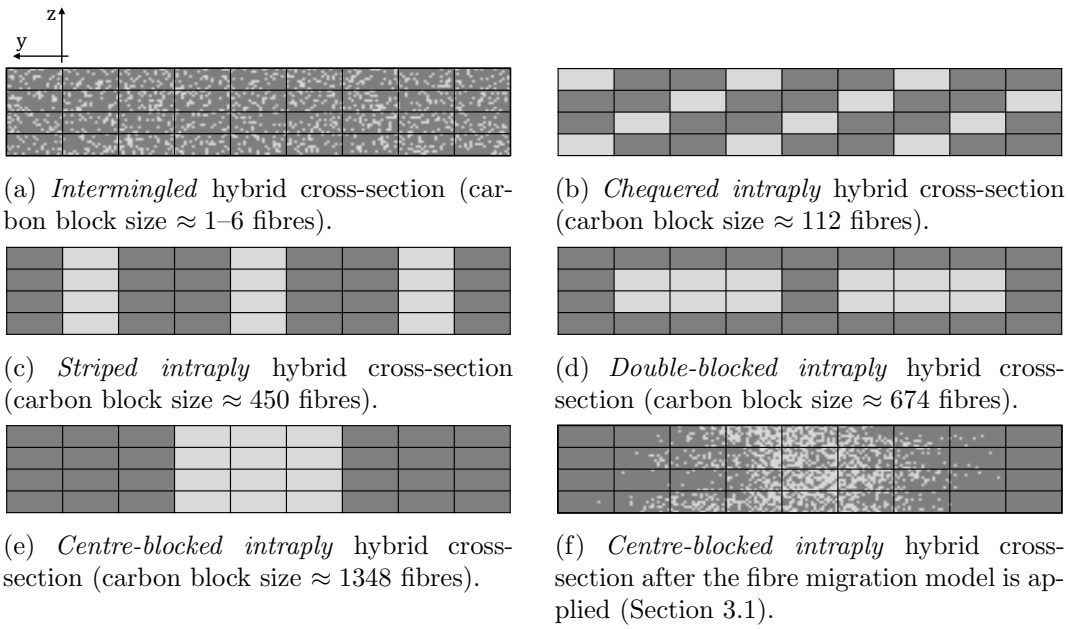

(a) *Intermingled* hybrid cross-section (carbon block size ≈ 1–6 fibres).

(b) *Chequered intraply* hybrid cross-section (carbon block size ≈ 112 fibres).

(c) *Striped intraply* hybrid cross-section (carbon block size ≈ 450 fibres).

(d) *Double-blocked intraply* hybrid cross-section (carbon block size ≈ 674 fibres).

(e) *Centre-blocked intraply* hybrid cross-section (carbon block size ≈ 1348 fibres).

(f) *Centre-blocked intraply* hybrid cross-section after the fibre migration model is applied (Section 3.1).

Figure 2: Different cross-section fibre arrangements investigated as part of this study (not to scale). Throughout this paper, glass fibres are shown in dark grey, while carbon fibres are shown in light grey (to match the fibres' appearance in micrographs).

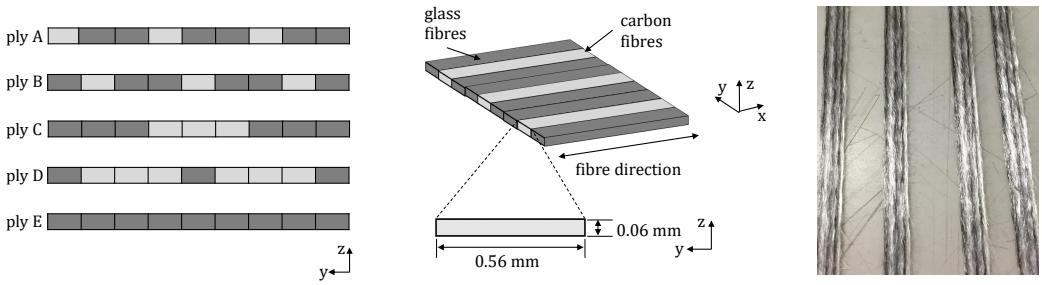

(a) Five distinct hybrid plies are made, which are combined to make the cross-sections shown in Figures 2b to 2e.

(b) In this paper, nine nozzles are used to create a ply with nine distinct sub-regions.

(c) Examples of several *striped intraply* hybrid plies.

Figure 3: The *intraply* HiPerDiF process shown in more detail for the *striped* fibre arrangement.

made using the HiPerDiF method.

2.3. Experimental testing

A schematic of the specimen used for tensile testing is shown in Figure 4. GFRP end-tabs were bonded with Huntsman Araldite 2014-1. Tensile tests were carried out using a servo-electric testing machine (Shimadzu, 10 kN, Japan) with a cross-head displacement speed of 1 mm/min. A white speckle pattern over a black background was painted on the specimens to allow strain measurement with a video extensiometer (IMETRUM, UK).

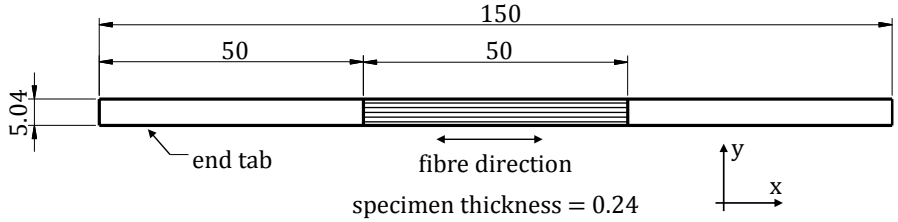

Figure 4: Specimen dimensions for experimental testing and analytical modelling. All dimensions are in mm.

Specimen cross-sections in epoxy pots were polished and prepared for microscopy analysis (Carl Zeiss, BG).

3. Model development

Stress vs. strain curves for the specimens described in Section 2 were modelled using a virtual testing framework with the fibre and matrix properties shown in Table 1. The virtual testing framework used in this paper was based on that recently proposed to model

intermingled hybrid discontinuous composites [10], but with two main modifications to account for the *intraply* (rather than *intermingled*) fibre arrangement, as described in Sections 3.1 and 3.2.

3.1. Model for realistic intraply fibre arrangements

The previously proposed *intermingled* model [10] arranged the fibres in a square cross-section, assuming a square fibre packing, and imposed a random arrangement of fibre types. The previous *intermingled* model was modified for this paper to enable a rectangular cross-section, of width w and thickness t; the rectangular cross-section changed the dimensions of the fibre type matrix ($\boldsymbol{T}$) from an n by n matrix to a $n_{\mathrm{f_i}}$ by $n_{\mathrm{f_j}}$ matrix, where $n_{\mathrm{f_i}}$ and $n_{\mathrm{f_j}}$ are the number of fibres across the thickness and width of the specimen:

$$n_{\mathrm{f_i}} = \mathrm{round}\left(\frac{t\sqrt{v_{\mathrm{f}}}}{\sqrt{\pi}\left(\frac{v_{\mathrm{c}}\phi_{\mathrm{c}}+(1-v_{\mathrm{c}})\phi_{\mathrm{g}}}{2}\right)}\right), \quad n_{\mathrm{f_j}} = \mathrm{round}\left(\frac{w\sqrt{v_{\mathrm{f}}}}{\sqrt{\pi}\left(\frac{v_{\mathrm{c}}\phi_{\mathrm{c}}+(1-v_{\mathrm{c}})\phi_{\mathrm{g}}}{2}\right)}\right). \tag{2}$$

The newly developed virtual testing framework was used to investigate the *intermingled*, *chequered*, *striped*, *double-blocked*, and *centre-blocked* fibre arrangements, which are shown in Figure 2. The intended *intraply hybrid* fibre arrangements were created in the virtual testing framework in a similar way to the experiments, by dividing the matrix of fibre types ($\boldsymbol{T}$) into $n_{\mathrm{r_i}} = 4$ by $n_{\mathrm{r_j}} = 9$ sub-regions, each with their own fibre type, as shown in Figure 5. Because different fibre types have different diameters, the number of fibres within each sub-region was selected to preserve the size (w_{r} and t_{r}) and fibre volume fraction (v_{f}) of each sub-region (as shown in Figure 5). The intended fibre arrangement was then stored in the matrix of fibre types ($\boldsymbol{T}$), where $\boldsymbol{T}^{[i,j]} = 0$ when fibre (i, j) is a glass fibre, and $\boldsymbol{T}^{[i,j]} = 1$ when fibre (i, j) is a carbon fibre.

It will be shown in Figures 8 to 12 that the intended fibre arrangements were significantly different from the fibre arrangements that were achieved in the experiments; this difference is because the fibres migrated from their intended position during the HiPerDiF manufacturing and alignment process. Consequently, once the intended fibre arrangement was stored in the matrix of fibre types ($\boldsymbol{T}$), an empirical 'fibre migration algorithm' was created to capture the movement of fibres types during the HiPerDiF process. This algorithm works by swapping carbon and glass fibres within $\boldsymbol{T}$, with the number of fibre swaps being governed by a 'fuzzy factor', ψ: a fuzzy factor of $\psi = 0$ implies no fibre migration, while a fuzzy factor of $\psi = 1$ implies that every carbon fibre has migrated some distance

around the cross-section.

The fibre migration algorithm follows the flowchart shown in Figure 6. For each swap of a carbon and glass fibre, the target location for each carbon fibre is defined by stochastic vertical and horizontal migrations:

- The vertical migration, Δi, is sampled from a normal distribution $\mathcal{N}\left(0, \sigma_{\mathrm{v}}^2\right)$, where σ_{v} is a pre-defined vertical migration standard deviation;
- The horizontal migration, Δj, is sampled from a normal distribution, $\mathcal{N}\left(\boldsymbol{\mu}_{\mathrm{h}}, \sigma_{\mathrm{h}}^2\right)$, where σ_{h} is a pre-defined horizontal migration standard deviation; $\boldsymbol{\mu}_{\mathrm{h}}$ is a stochastic vector of mean horizontal migrations, which are defined independently for every couple of lines in the matrix $\boldsymbol{T}$, and which are sampled from a random distribution defined as $\mathcal{U}\left(-0.5m_{\mathrm{h}}, +0.5m_{\mathrm{h}}\right)$, where m_{h} is a pre-defined maximum horizontal migration interval.

This process is repeated until the correct level of fibre migration (defined by the migration "fuzzy factor" ψ) is achieved. Figure 7 shows the cumulative effects of the various features of the fibre migration algorithm.

The inputs for the fibre migration algorithm were adjusted empirically until the experimental fibre arrangements visually matched with the migrated fibre arrangements (seen by comparing Figures 8b to 12b with Figures 8c to 12c). The inputs for the fibre migration algorithm are normalised by the relative dimensions of the cross-section ($n_{\mathrm{f_i}} = 18$ fibres and $n_{\mathrm{f_j}} = 387$ fibres) and of the sub-regions ($n_{\mathrm{r_i}} = 4$ sub-regions and $n_{\mathrm{r_j}} = 9$ sub-regions), as shown in Table 2.

Table 2: Inputs for the fibre migration algorithm for the four *intraply* hybrid cross-sections.

Cross-section	σ_{v}	m_{h}	σ_{h}	ψ
Chequered	$n_{\mathrm{f_i}}/\left(4n_{\mathrm{r_i}}\right) = 1.125$	$2n_{\mathrm{f_j}}/n_{\mathrm{r_j}} = 86$	$3n_{\mathrm{f_j}}/\left(4n_{\mathrm{r_j}}\right) = 32.25$	0.96
Striped	$n_{\mathrm{f_i}}/\left(4n_{\mathrm{r_i}}\right) = 1.125$	$2n_{\mathrm{f_j}}/n_{\mathrm{r_j}} = 86$	$3n_{\mathrm{f_j}}/\left(4n_{\mathrm{r_j}}\right) = 32.25$	0.96
Double-blocked	$n_{\mathrm{f_i}}/\left(4n_{\mathrm{r_i}}\right) = 1.125$	$2n_{\mathrm{f_j}}/n_{\mathrm{r_j}} = 86$	$3n_{\mathrm{f_j}}/\left(4n_{\mathrm{r_j}}\right) = 32.25$	0.80
Centre-blocked	$n_{\mathrm{f_i}}/\left(4n_{\mathrm{r_i}}\right) = 1.125$	$2n_{\mathrm{f_j}}/n_{\mathrm{r_j}} = 86$	$3n_{\mathrm{f_j}}/\left(4n_{\mathrm{r_j}}\right) = 32.25$	0.80

3.2. Fracture-based failure criterion for intermingled and intraply hybrid composites

The average stress-strain curve of hybrid discontinuous composites can be predicted using a previously-developed virtual testing framework [10]. This framework decomposes a complete composite specimen into Representative Volume Elements (RVEs), each with the

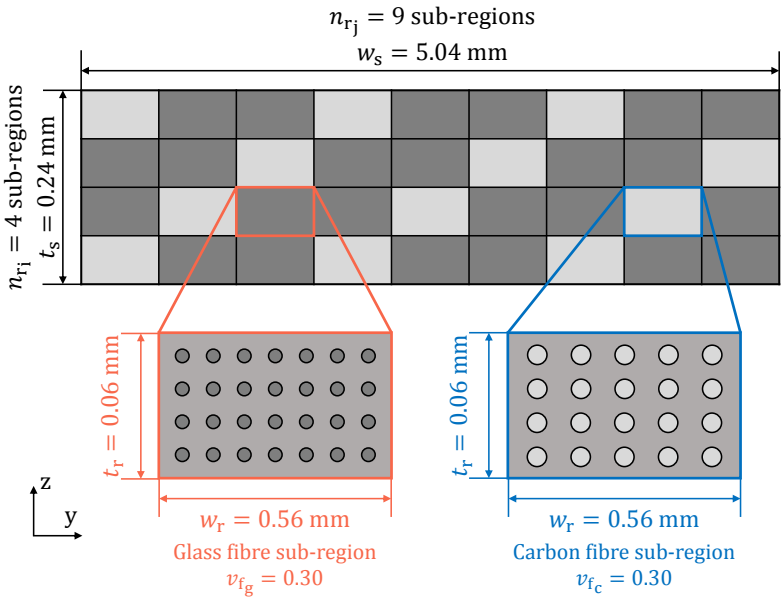

Figure 5: Definition of the sub-regions (intended to have a single fibre type) within a virtual specimen cross-section. Different fibres have a different diameter, therefore the sub-regions are all the same physical size (t_r = 0.06 mm and w_r = 0.56 mm) and have the same overall fibre volume fraction (v_f = 0.30), but the number of fibres within the sub-region varies by fibre type.

length of one fibre and a full specimen cross-section. The stress-strain curve for each RVE is then analysed individually, assuming a shear-lag stress transfer between neighbouring fibres (considering the random location of fibre-ends, and matrix non-linearity and failure), and allowing for fibre fragmentation (governed by Weibull fibre-strength distributions). Full details of the virtual testing framework and its application to *intermingled* hybrid discontinuous composites are provided elsewhere [10].

The virtual testing framework for *intermingled* discontinuous composites [10, 19] proposed that the full stress-strain curve of a hybrid discontinuous composite specimen can be calculated by combining the stress-strain curves of its individual RVEs in series. Subsequently, a non-linear fracture mechanics criterion is used to determine the ultimate strength and failure strain of the specimen; this criterion aims to model unstable fracture of an entire cross-section, triggered by the formation of a broken-fibre cluster of a critical size. To do so, the criterion first identifies the weakest square-shaped cluster of a given size within the specimen; fracture will occur if the strain energy release rate of the corresponding penny-shaped crack is greater than the average fracture toughness of the composite; if not, then the size of the square cluster is increased, until fracture is predicted.

Henry and Pimenta's fracture-based failure criterion mentioned above [10, 19] works

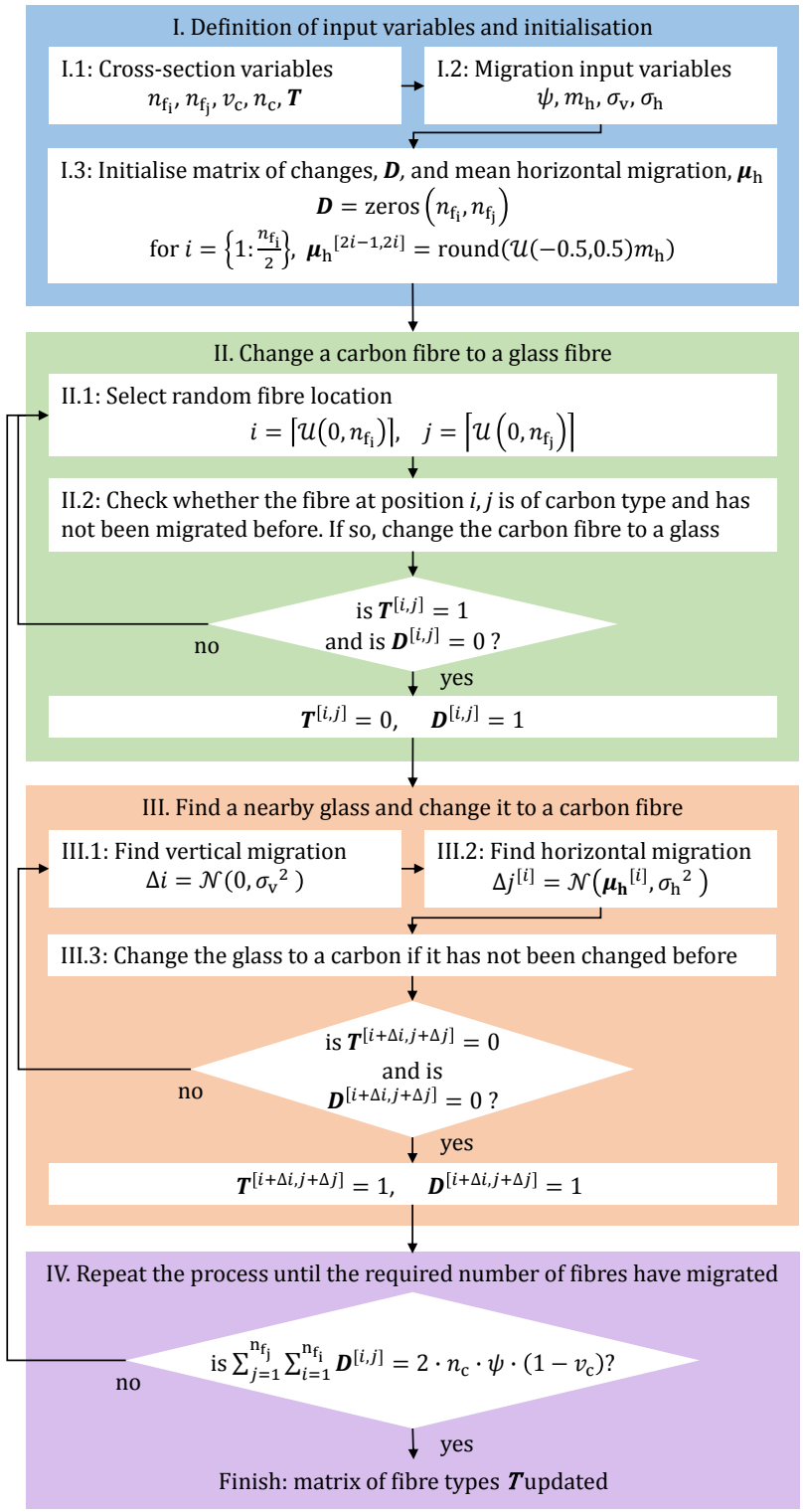

Figure 6: Flow chart of the fibre migration algorithm.

(a) Intended *double-blocked* cross-section; $\sigma_{\mathrm{v}} = 0$, $m_{\mathrm{h}} = 0$, and $\sigma_{\mathrm{h}} = 0$.

(b) *Double-blocked* cross-section with only a vertical migration applied. The vertical migration introduces vertical spread in the fibre location; $\sigma_{\mathrm{v}} = 1.125$, $m_{\mathrm{h}} = 0$, and $\sigma_{\mathrm{h}} = 0$.

(c) *Double-blocked* cross-section with a vertical migration, and a row-based horizontal migration applied. The row-based horizontal migration introduces the layered effect in the cross-section; $\sigma_{\mathrm{v}} = 1.125$, $m_{\mathrm{h}} = 86$, and $\sigma_{\mathrm{h}} = 0$.

(d) *Double-blocked* cross-section with a vertical migration, a row-based horizontal migration, and a fibre-based horizontal migration applied. The fibre-based migration introduces horizontal spread into the cross-section; $\sigma_{\mathrm{v}} = 1.125$, $m_{\mathrm{h}} = 86$, and $\sigma_{\mathrm{h}} = 32.25$.

Figure 7: *Double-blocked* cross-sections showing the cumulative effects of each aspect of the fibre migration algorithm.

(a) Intended *intermingled* cross-section.

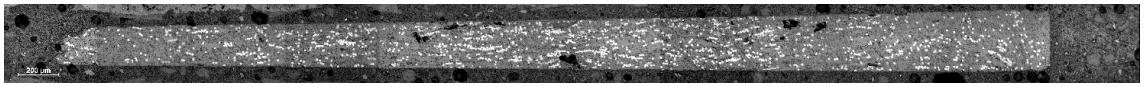

(b) Experimental *intermingled* cross-section.

(c) *Intermingled* cross-section (note that for the *intermingled* case only, zero migration occurs as the cross-section is already intermingled). The critical cluster is also highlighted.

Figure 8: The intended *intermingled* cross-section, the experimental cross-section after manufacture, and the cross-section after the fibre migration model was applied. Small critical clusters are formed before fracture of the *intermingled* specimen (Section 4.1).

(a) Intended *chequered* cross-section.

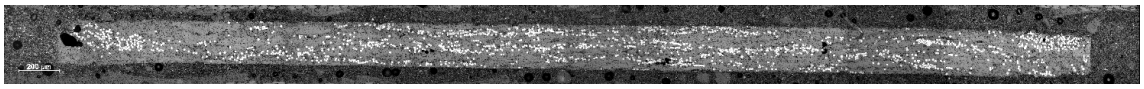

(b) Experimental *chequered* cross-section.

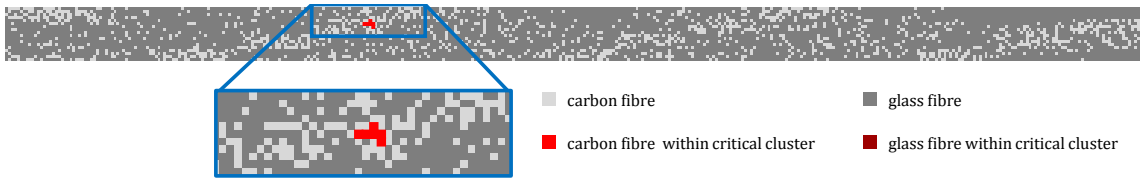

(c) *Chequered* cross-section with fibre migration model applied. The critical cluster is also highlighted.

Figure 9: The intended *chequered* cross-section, the experimental cross-section after manufacture, and the cross-section after the fibre migration model was applied. Medium-sized critical clusters are formed before fracture of the *chequered* specimen (Section 4.1).

(a) Intended *striped* cross-section.

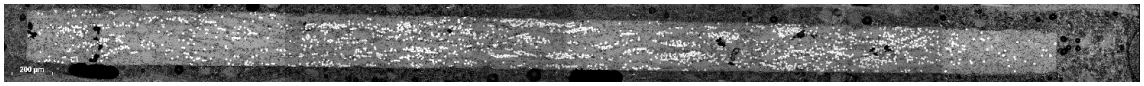

(b) Experimental *striped* cross-section.

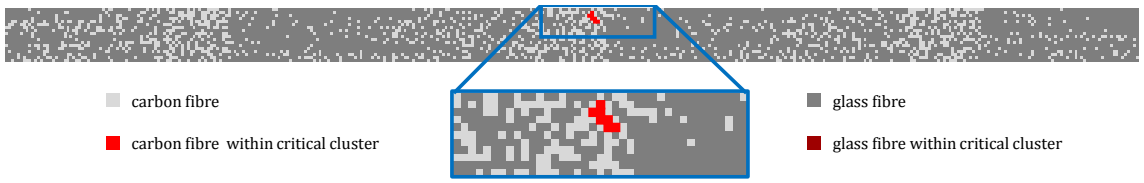

(c) *Striped* cross-section with fibre migration model applied. The critical cluster is also highlighted.

Figure 10: The intended *striped* cross-section, the experimental cross-section after manufacture, and the cross-section after the fibre migration model was applied. Medium-sized critical clusters are formed before fracture of the *striped* specimen (Section 4.1).

(a) Intended *double-blocked* cross-section.

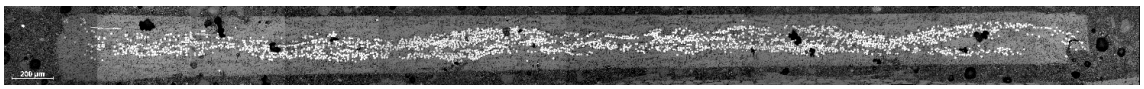

(b) Experimental *double-blocked* cross-section.

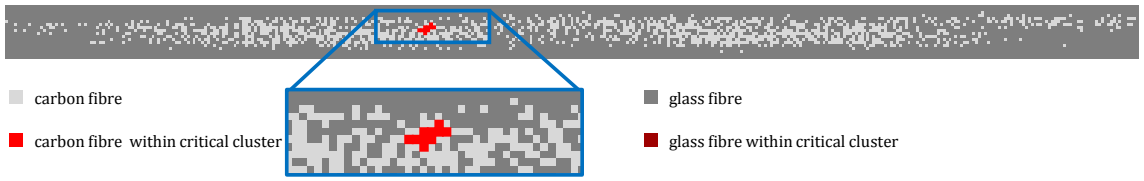

(c) *Double-blocked* cross-section with fibre migration model applied. The critical cluster is also highlighted.

Figure 11: The intended *double-blocked* cross-section, the experimental cross-section after manufacture, and the cross-section after the fibre migration model was applied. Medium critical clusters are formed before fracture of the *double-blocked* specimen (Section 4.1).

(a) Intended *centre-blocked* cross-section.

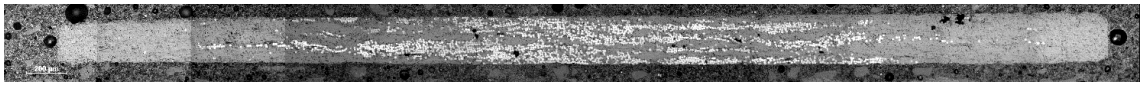

(b) Experimental *centre-blocked* cross-section.

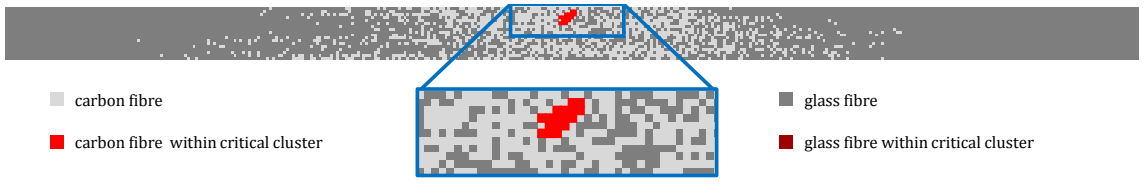

(c) *Centre-blocked* cross-section with fibre migration model applied. The critical cluster is also highlighted.

Figure 12: The intended *centre-blocked* cross-section, the experimental cross-section after manufacture, and the cross-section after the fibre migration model was applied. Large critical clusters are formed before fracture of the *centre-blocked* specimen (Section 4.1).

well for non-hybrid discontinuous composites, and for hybrid discontinuous composites with *intermingled* cross-sections. Although it is recognised that a square cluster may contain unbroken fibres or may neglect adjacent broken fibres, the effects of these two assumptions will effectively cancel one-another out for an *intermingled* cross-section, due to the random fibre arrangement; however, these effects will be much more significant for *intraply* hybrids, as the cross-section is more ordered. In an *intraply* hybrid, the propagation of failure from a given cluster will also be associated with a fracture toughness that is dependent on the properties of the fibres surrounding that broken cluster, something that is also neglected in Henry and Pimenta's method for *intermingled* hybrids [10, 19].

We thus propose an improved fracture-based failure criterion (see the flowchart in Figure 13), which accurately calculates the size, shape, position, and fracture toughness associated with clusters of broken fibres; this fracture criterion is therefore suited for both *intermingled* and *intraply* hybrid discontinuous composites. In order to determine the fracture-based failure strain, the following steps are carried out for every RVE:

- Inputs for the fracture criterion are first gathered; this includes the matrix of fibre types ($\boldsymbol{T}$, from Section 3.1), full RVE stress-strain curve ($\boldsymbol{\sigma}_{\mathrm{RVE}}$ vs. $\boldsymbol{\varepsilon}_{\mathrm{RVE}}$), matrix of fibre stresses ($\boldsymbol{\sigma}_{\mathrm{f}}$), RVE initial stiffness (E_{RVE}), and the ultimate strength of the RVE (X_{RVE}, from Henry and Pimenta [10], without considering the possibility of unstable fracture).

- At each strain increment ($\boldsymbol{\varepsilon}_{\mathrm{RVE}}$), all fully-failed fibres (which carry zero stress due to either fibre fragmentation or matrix debonding) are identified and stored in the matrix of failed fibres $\boldsymbol{B}$. Clusters of fibre breaks are identified using the 'bwlabel' function in MATLAB (see Figure 14 for details).

- The fracture toughness of the material surrounding each cluster is determined (see Appendix A). For each of the n_{k} clusters of broken fibres, the equivalent penny-shape crack radius is determined, and the associated strain energy release rate is calculated. The fracture stress of the RVE is then determined when the maximum strain energy release rate $\boldsymbol{J}$ (associated with fracture propagating from the most critical cluster) exceeds the fracture toughness $\mathcal{G}_{\mathrm{I}}$ of the material surrounding the critical cluster.

- This process is repeated for all of the RVEs and the minimum fracture strength of all the RVEs is determined.

Once this process is repeated for every RVE, the specimen stress-strain curve is formed from the average of all of the RVE stress-strain curves. The specimen stress-strain curve is then trimmed up to the minimum fracture strength.

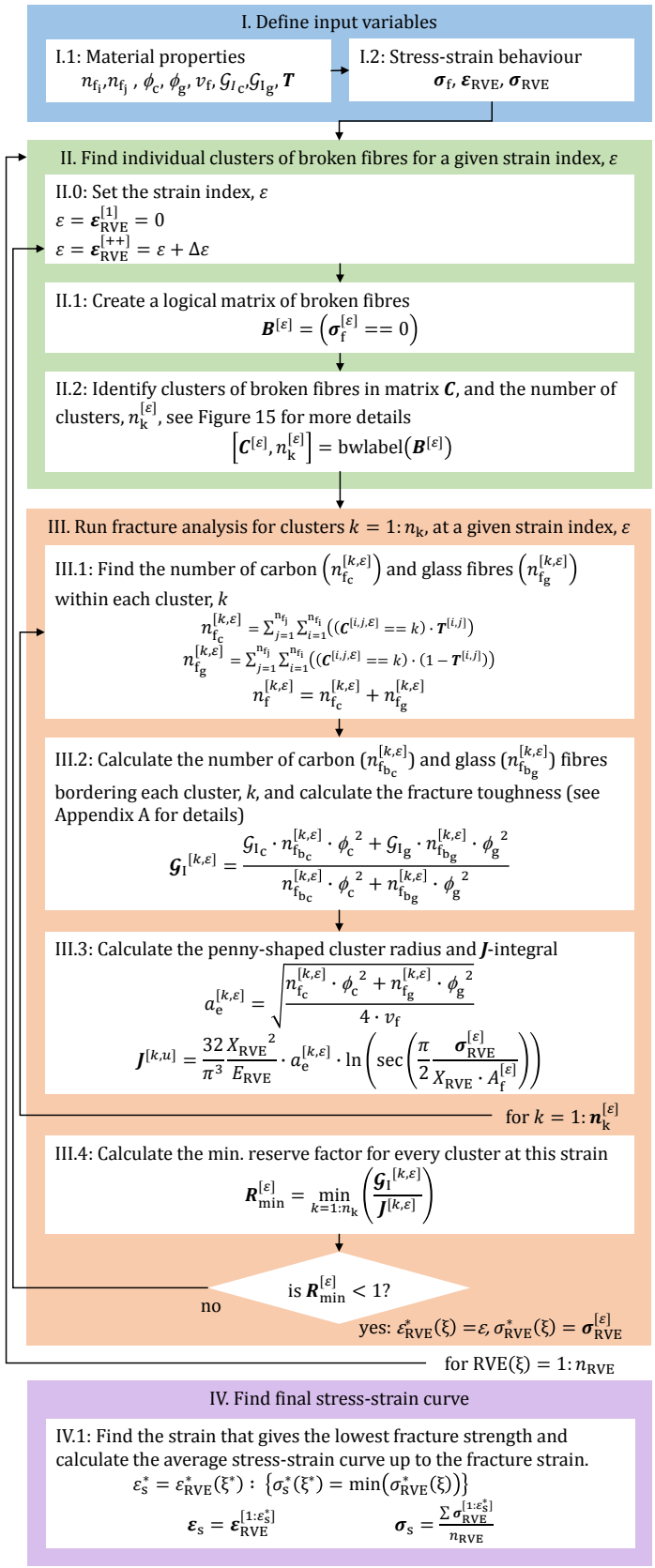

Figure 13: Flow chart to demonstrate the implementation of the fracture-based failure criterion. The 'bwlabel' function is shown in further detail in Figure 14, along with the '==' symbol, which denotes the logical operation 'if equal to'.

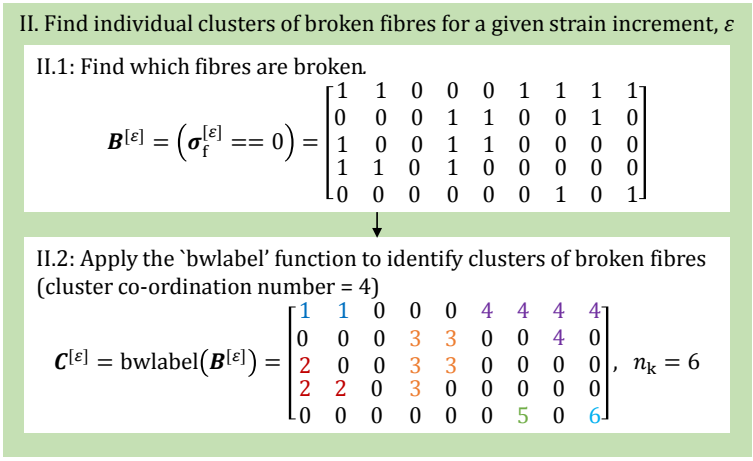

Figure 14: Flow chart which shows an example of the "bwlabel" function in practice. The "bwlabel" function finds failed fibres that also have neighbouring failed fibres to the top, bottom, left, or right of themselves, and numbers each cluster with a unique identifier. The "bwlabel" function is used in MATLAB code and can be found in the documentation [25].

4. Results and discussion

4.1. Model validation

The stress-strain curves for the experiments and virtual testing framework predictions are in good agreement, as can be seen in Figure 15. Due to the stochastic assignment of fibre types, fibre ends, and fibre strengths, outputs from the virtual testing framework are stochastic; consequently, three model runs are shown for each fibre arrangement (the same as the number of experimental runs), with the point of fracture for each model run marked with a red cross. Although the model was only run for a small number of times, the results indicate a similar level of variability between the virtual testing framework and the experiments.

The level of fibre alignment in the experimental specimens was not measured, although the HiPerDiF method has previously shown that very good levels of fibre alignment can be achieved [5], and the effects of fibre misalignment from the HiPerDiF method have been proven to be small [26]. This evidence, coupled with good correlation between the initial stiffness of the experimental and modelling curves, suggests that the level of fibre misalignment in the specimens was negligible, and had little or no effect on the structural performance of the manufactured specimens.

The virtual testing framework over-predicts the initial stiffness and pseudo-yield strength of the *centre-blocked* fibre arrangement; a significant load drop is also predicted that is not shown in the experiments (Figure 15e). The high initial stiffness indicates that there might

be a lower number of carbon fibres in the experimental tests than in the model, as the carbon fibres are much stiffer than the glass fibres; a higher number of carbon fibres also leads to a larger load drop, as more of the low elongation fibres will fragment at low strain. The model is therefore re-run in Figure 15f) for a carbon ratio of $v_c = 0.28$ to reduce the number of carbon fibres within the cross-section, which gives a much better agreement for the pseudo-yield strength, initial stiffness, and load drop behaviour for both experiments and modelling. Another possible reason for this lower initial stiffness in the *centre-blocked* fibre arrangement may be due to poorer alignment of the carbon fibres when large groups of these fibres are formed, as previously discussed by Yu et al. [9]; however, this is unlikely to be the case, because a significant level of fibre misalignment would also lead to a strain hardening initial response (due to the re-alignment of the fibres with increasing strain), which was not seen in the experiments. Poor control of the carbon ratio or HMC fibre alignment may explain why there is also a small mismatch between the stiffness and load-drop of the experimental and modelling results for the *double-blocked* fibre arrangement in Figure 15d.

Figures 8c to 12c and Figure 15 indicate that fibre arrangements with the coarsest fibre-type grouping (i.e. the *double-bocked* and *centre-blocked* cross-sections) have a lower strength and strain to failure. This is because larger clusters of broken fibres promote overall fracture of the specimen at lower strains, because the cluster strain energy release rate (Stage III.3 of Figure 13) increases significantly with cluster size. The strength and failure strain of a hybrid discontinuous composite material could therefore be improved by maximising the level of intermingling within the cross-section, as intermingling will reduce the size of the low elongation fibre groups and, consequently, will delay the formation of large broken clusters.

The modifications to the virtual testing framework proposed in this paper are essential in order to accurately model *intraply* hybrid discontinuous composites. Without the application of the fibre migration algorithm, the virtual testing framework predicts a brittle stress-strain response for the *intraply centre-blocked* cross-section (Figure 16a), while in reality a small amount of ductility was observed during the experiments. The proposed fracture criterion is also necessary to predict an accurate failure strain of the *intraply* fibre arrangements (Figure 16b).

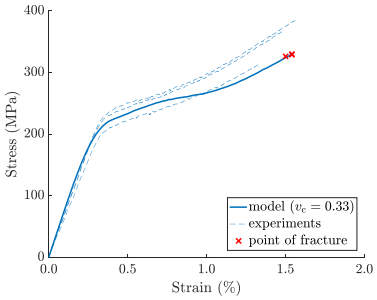

(a) Stress-strain curve for the *intermingled* cross-section.

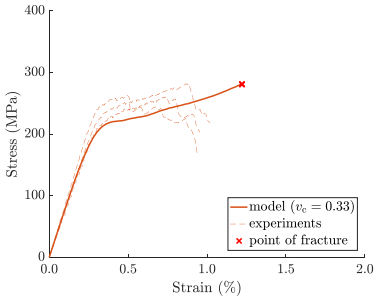

(b) Stress-strain curve for the *chequered* cross-section.

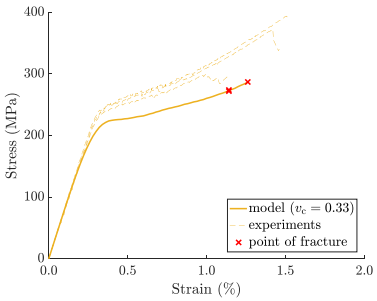

(c) Stress-strain curve for the *striped* cross-section.

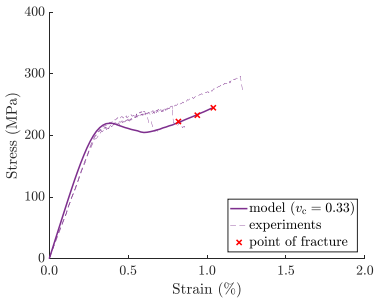

(d) Stress-strain curve for the *double-blocked* cross-section.

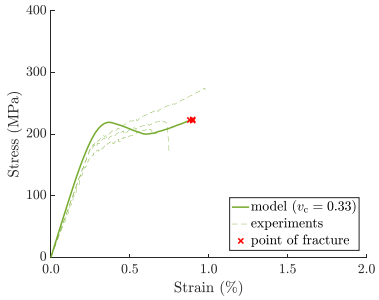

(e) Stress-strain curve for the *centre-blocked* cross-section.

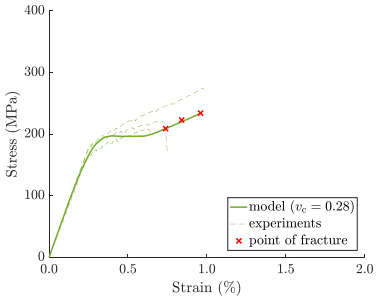

(f) Stress-strain curve for the *centre-blocked* cross-section with the carbon ratio scaled to match experiments.

Figure 15: Stress-strain curves for the various hybrid cross-section arrangements.

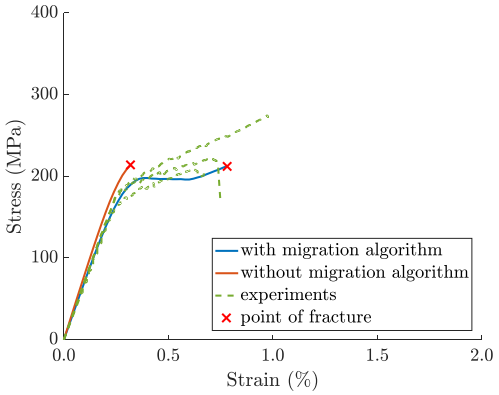

(a) Stress-strain curve for the *centre-blocked* cross-section with and without the migration model applied.

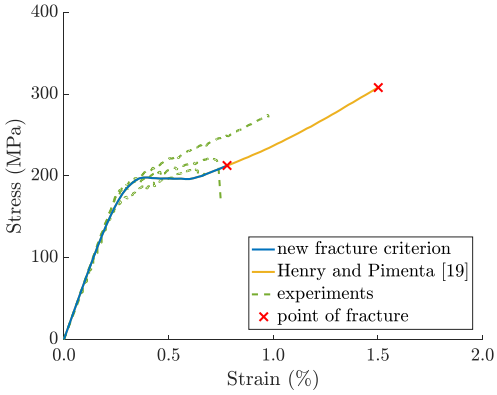

(b) Stress-strain curve for the *centre-blocked* cross-section, with two different fracture-based failure criterion applied.

Figure 16: Two sets of stress-strain curves demonstrating the importance of the proposed fibre migration algorithm and the proposed fracture-based failure criterion for the *centre-blocked* cross-section.

4.2. Effect of intermingling

Increasing levels of random intermingling (i.e. randomly swapping carbon and glass fibres within the cross-section) were applied to the *centre-blocked* cross-section, which resulted in smaller groups of low elongation fibres (see Figure 17). Smaller groups of low elongation fibres caused smaller clusters of fibre breaks to form, because the fragmented low elongation fibres remained more isolated from one-another. Increasing intermingling is therefore an effective means to increase the strength and pseudo-ductility of hybrid discontinuous composites (see Figure 18), as the critical cluster size and resulting strain energy release rate is kept small.

(a) A large critical cluster is formed when a low level of intermingling (20%) is applied.

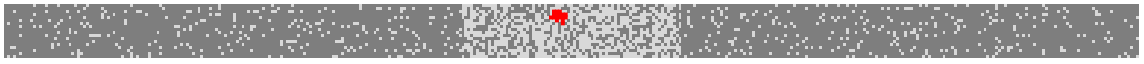

(b) A medium-sized critical cluster is formed when a medium level of intermingling (60%) is applied.

(c) A small critical cluster is formed when a high level of intermingling (100%) is applied.

Figure 17: The *centre-blocked* microstructure with increasing levels of random intermingling. Increasing levels of intermingling reduces the size of the critical cluster (shown in red) before fracture. The size of the critical cluster can be minimised by isolating low elongation fibres from one-another.

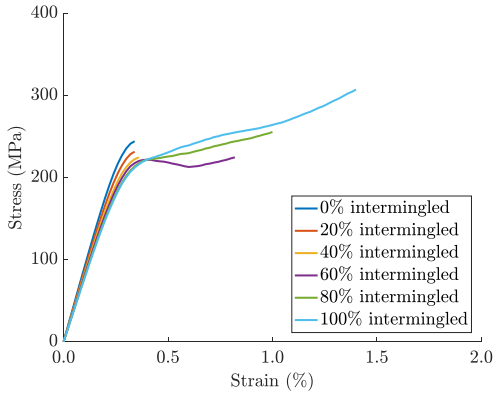

Figure 18: Effect of increasing intermingling on the stress-strain curve of *intraply* hybrid discontinuous composites with a *centre-blocked* microstructure. Increasing intermingling results in an increase in pseudo-yield strength, ultimate strength, and pseudo-ductile strain, but a reduction in initial stiffness.

It should be noted that the *centre-blocked* cross-section with the least intermingling ($\psi = 0$) showed the highest initial modulus (as also shown in Figures 15a to 15f and Figure 18). Henry and Pimenta [26] showed that the maximum modulus in a hybrid discontinuous composite is achieved when the stiffnesses of the interacting (i.e. neighbouring) fibres are similar to one-another. The modulus of the whole specimen is therefore maximised when the fibre types are arranged such that those interactions mainly consist of the same fibre type (i.e. when intermingling is minimised). Intermingling therefore presents a clear trade-off between (i) strength and pseudo-ductility or (ii) stiffness, although the positive effect of intermingling on the strength and ductility appears to be much more significant than the negative effect on stiffness (for the fibre diameters and stiffnesses considered here).

4.3. Quantifying the effect of fibre-type grouping using controlled fibre arrangements

Several fibre arrangements with controlled levels of intermingling (shown in Figure 19) were investigated using the virtual testing framework, in order to quantify how grouping low elongation fibres influences the structural performance of hybrid discontinuous composites. The *isolated fibre* cross-section features single carbon fibres that are surrounded entirely by glass fibres, in order to minimise the size of clusters of broken fibres and delay fracture for as long as possible. The *4-block*, *9-block*, *16-block*, and *25-block* cross-sections feature increasingly large groups of low-elongation carbon fibres, so that the influence of fibre grouping could be quantified. Finally, the *thin-ply* fibre arrangement features layers of single carbon fibres across the entire width of the cross-section; this cross-section was

suggested by Swolfs et al. [14] to maximise the hybrid effect for the failure strain of the low elongation fibres. It should be noted that carbon fibres were added randomly to the *thin-ply* cross-section in order to maintain a consistent carbon ratio ($v_c = 0.33$) with the other fibre arrangements.

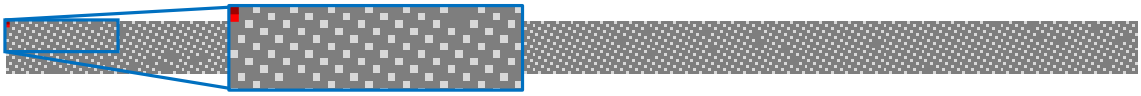

(a) The *isolated fibre* fibre arrangement.

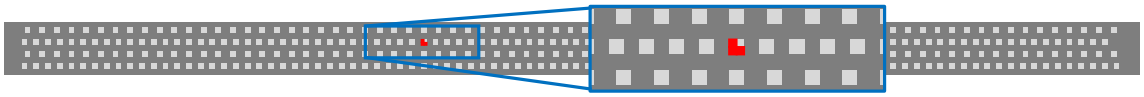

(b) The *4-block* fibre arrangement.

(c) The *9-block* fibre arrangement.

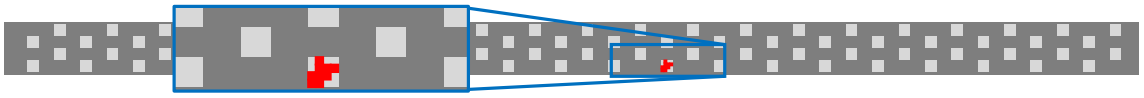

(d) The *16-block* fibre arrangement.

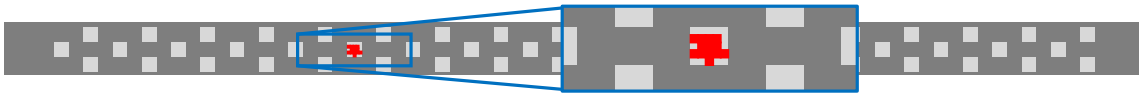

(e) The *25-block* fibre arrangement.

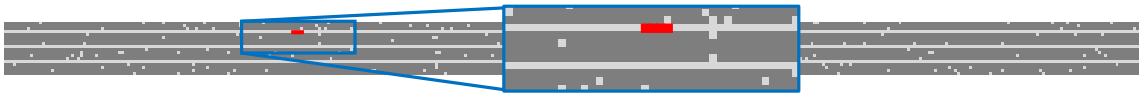

(f) The *thin-ply* fibre arrangement. Please note that carbon fibres were added randomly to the *thin-ply* cross-section in order to maintain a consistent carbon ratio ($v_c = 0.33$) with the other fibre arrangements.

Figure 19: Highly controlled fibre arrangements for detailed analysis of the effects of fibre-type grouping.

Pseudo-ductile strains were calculated for all fibre arrangements using the method proposed by Wisnom et al. [27], while pseudo-yield strengths were calculated using a 0.1% strain offset. Using these methods the *isolated fibre* arrangement demonstrates the optimal structural performance, with a 27% increase in ultimate strength, a 21% increase in pseudo-yield strength, and a 44% increase in pseudo-ductile strain when compared to the *intermingled* fibre arrangement (see Figure 20). The critical cluster in the *isolated*

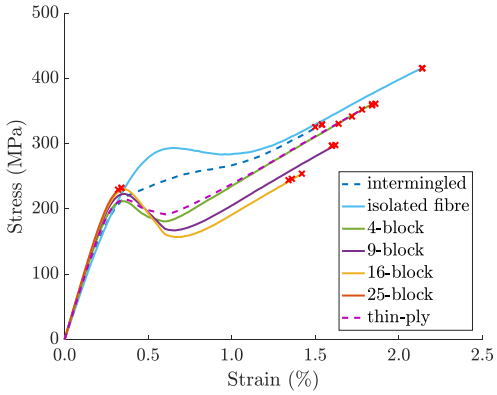

Figure 20: A comparison between the stress-strain curves of the *intermingled* and highly controlled fibre-arrangements. If the low elongation fibres are isolated from one another (i.e. if the *isolated fibre* arrangement is used), the pseudo-yield strength, ultimate strength, and pseudo-ductile strain are maximised, with a minor reduction in stiffness.

fibre arrangement contains a single carbon and a single glass fibre (see Figure 19a), which indicates that the isolated fibre arrangement successfully prevents clusters of broken low elongation fibres from merging with one-another. By keeping clusters to a minimum size, the strain energy release rate of the critical cluster is kept to a minimum, therefore the the maximum strength and pseudo-ductility is reached in the hybrid discontinuous composite material.

The initial modulus increases for the more highly-grouped fibre arrangements (Figure 20), with the *25-block* fibre arrangement showing the largest modulus increase of 18% relative to the *isolated fibre* arrangement; this modulus increase is in line with observations in Section 4.2. However, the more highly-grouped fibre arrangements also show significantly lower ultimate strength, pseudo-ductility, and pseudo-yield strength as the size of the fibre groups increases; the most significant case is the *25-block* fibre arrangement, which shows an almost brittle response, a 44% reduction in ultimate strength, and a 96% reduction in pseudo-ductile strain, relative to *isolated fibre* arrangement. Larger groups of low elongation fibres enable larger clusters of broken fibres to form (as shown in Figures 19b to 19d), hence fracture occurs at increasingly lower strains, as mentioned in Section 4.1.

The *intermingled*, *4-block*, and *thin-ply* arrangements all show similar critical cluster sizes, ultimate strengths, and failure strains, however the *4-block*, and *thin-ply* arrangements feature a significant load-drop after yielding (Figure 20). When a fibre breaks, the stress from the broken fibre is passed to the neighbouring fibres; therefore, failure of the

low elongation fibres generates significantly higher stress concentrations in neighbouring low elongation fibres than in neighbouring high elongation fibres, due to the larger diameter and modulus of the low elongation fibres. These higher stress concentrations lead to further failures of low elongation failures propagating through the whole specimen, which leads to a significant global load drop. For the fibre types considered in this study, intermingling is an effective way to prevent the propagation of fibre breaks, as it results in more of the fibre breaks being shielded by high elongation fibres; these high-elongation fibres are not only less susceptible to breaking at low applied strains, but they also experience a lower stress concentration and hence are less likely to fail in the vicinity of a fibre break. It should be noted that this argument does not hold when the hybrid reinforcements have equal diameters; in this case the thin ply has a higher ultimate strength pseudo-ductile strain than the intermingled case, in line with predictions made by Swolfs et al. [14], however the *isolated fibre* arrangement remains the strongest and most ductile.

5. Conclusion

This paper combines experiments and a virtual testing framework to explore how grouping low elongation fibres affects the pseudo-ductility of aligned hybrid discontinuous composites. The main conclusions are shown below:

- Both *intermingled* and *intraply* aligned hybrid discontinuous composite materials were successfully manufactured using an improved High Performance Discontinuous Fibre (HiPerDiF) method.
- Significant migration of the fibres was present during the *intraply* HiPerDiF process. A new fibre migration model was therefore developed to simulate fibre migration in the virtual testing framework; the migration algorithm was proven to be essential in order for the virtual testing framework to capture the correct stress-strain response of the *intraply* hybrid discontinuous composites.
- A new fracture criterion was also developed for the virtual testing framework, in order to predict final failure of both *intermingled* and *intraply* hybrids. The proposed fracture criterion proved to be necessary for an accurate prediction of the failure strain of *intraply* aligned hybrid discontinuous composites.
- Both the experiments and the new virtual testing framework indicated that the *intermingled* fibre arrangement had the highest strength and pseudo-ductility out

of the arrangements tested in the experiments; the *intermingled* fibre arrangement was successful because it featured small groups of low elongation fibres, which delayed fracture by preventing large clusters of broken fibres from forming. These results suggest that the HiPerDiF process is the current state-of-the-art manufacturing method for maximising pseudo-ductility in hybrid discontinuous composites, because the HiPerDiF process produces the most dispersed fibre-type intermingling of all manufacturing processes for hybrid composites in the literature so far [11, 16].

- A further theoretical study using the virtual testing framework showed that a cross-section with full-scale isolation of low elongation fibres could present a further improvement on the strength and ductility of the *intermingled* fibre arrangement. A 27% increase in ultimate strength, a 21% increase in pseudo-yield strength, and a 44% increase in pseudo-ductile strain were achieved for the *isolated fibre* arrangement when compared to the *intermingled* arrangement.

The qualitative conclusions drawn in this paper are valid for any hybrid discontinuous material system where the failure strains of the two fibres are dissimilar and the ratio between the two fibre types is adequately selected. High modulus / high strength carbon hybrid discontinuous composites would qualitatively agree with the conclusions drawn here, although the virtual testing framework would have to be re-used with the correct inputs for those two fire-types, in order to quantify any changes in overall strength and ductility of the materials. The virtual testing framework developed in this paper is capable of modelling a large variety of material systems; this framework will therefore be used to further investigate different hybrid (or non-hybrid) fibre types, fibre volume fractions, matrix behaviours, and fibre arrangements to find an optimal material for strength and pseudo-ductility. One example of this Future work will also look at optimising the strength and ductility of aligned hybrid discontinuous composites by implementing an *isolated fibre* arrangement using the HiPerDiF method and by using higher fibre volume fractions.

6. Acknowledgements

This work was funded under the UK Engineering and Physical Sciences Research Council (EPSRC) programme grant EP/I02946X/1 on *High Performance Ductile Composite Technology*. S. Pimenta acknowledges the support from the Royal Academy of Engineering for her Research Fellowship on *Multiscale discontinuous composites for large scale and*

sustainable structural applications (2015-2019).

All underlying data to support the conclusions are provided within this paper.

7. References

[1] Anil N. Netravali and Shitij Chabba. Composites get greener. *Materials Today*, 6(4):22–29, apr 2003.

[2] Bernard L. Koff. Gas Turbine Technology Evolution: A Designers Perspective. *Journal of Propulsion and Power*, 20(4):577–595, jul 2004.

[3] Soraia Pimenta and Paul Robinson. An analytical shear-lag model for composites with brick-and-mortar' architecture considering non-linear matrix response and failure. *Composites Science and Technology*, 104:111–124, nov 2014.

[4] Gergely Czél, Soraia Pimenta, Michael R. Wisnom, and Paul Robinson. Demonstration of pseudo-ductility in unidirectional discontinuous carbon fibre/epoxy prepreg composites. *Composites Science and Technology*, 106:110–119, 2015.

[5] HaNa Yu, Kevin D. Potter, and Michael R. Wisnom. A novel manufacturing method for aligned discontinuous fibre composites (High Performance-Discontinuous Fibre method). *Composites Part A: Applied Science and Manufacturing*, 65:175–185, 2014.

[6] Yentl Swolfs, Larissa Gorbatikh, and Ignaas Verpoest. Fibre hybridisation in polymer composites: A review. *Composites Part A: Applied Science and Manufacturing*, 67:181–200, 2014.

[7] Meisam Jalalvand, Gergely Czél, and Michael R. Wisnom. Damage analysis of pseudo-ductile thin-ply UD hybrid composites A new analytical method. *Composites Part A: Applied Science and Manufacturing*, 69:83–93, 2015.

[8] Meisam Jalalvand, Gergely Czél, and Michael R. Wisnom. Parametric study of failure mechanisms and optimal configurations of pseudo-ductile thin-ply UD hybrid composites. *Composites Part A: Applied Science and Manufacturing*, 74:123–131, 2015.

[9] HaNa Yu, Marco L. Longana, Meisam Jalalvand, Michael R. Wisnom, and Kevin D. Potter. Pseudo-ductility in intermingled carbon/glass hybrid composites with highly aligned discontinuous fibres. *Composites Part A: Applied Science and Manufacturing*, 73:35–44, 2015.

[10] Joël Henry and Soraia Pimenta. Prediction of Mechanical Properties of Hybrid Discontinuous Composites. In *ECCM17 - 17th European Conference on Composite Materials*, pages 1–7, Munich, Germany, 2016.

[11] Peter W. Manders and M. G. Bader. The strength of hybrid glass/carbon fibre composites. *Journal of Materials Science*, 16(8):2233–2245, aug 1981.

[12] Peter W. Manders and M. G. Bader. The strength of hybrid glass/carbon fibre composites Part 2 A statistical mode. *Journal of Materials Science*, 16:2246–2256, 1981.

[13] Young-Jun You, Young-Hwan Park, Hyeong-Yeol Kim, and Ji-Sun Park. Hybrid effect on tensile properties of FRP rods with various material compositions. *Composite Structures*, 80(1):117–122, 2007.

[14] Yentl Swolfs, Robert M. McMeeking, Ignaas Verpoest, and Larissa Gorbatikh. The effect of fibre dispersion on initial failure strain and cluster development in unidirectional carbon/glass hybrid composites. *Composites Part A: Applied Science and Manufacturing*, 69:279–287, 2015.

[15] Don Lee and Jeffrey Satterwhite. Study of notch sensitivity of carbon-glass intraply laminates for aerospace applications. In *ICCM 19 - The 19th International Conference on Composite Materials*, pages 1–9, Montreal, Canada, 2013.

[16] Hele Diao, Alexander Bismarck, Paul Robinson, and Michael R. Wisnom. Production of continuous intermingled CF/GF hybrid composite via fibre tow spreading technology. In *ECCM16 - 16th European Conference on Composite Materials*, pages 1–8, Seville, Spain, 2014.

[17] HaNa Yu, Marco L. Longana, Nick Salavati, and Kevin D. Potter. Analysis of aligned short fibre preforms by the HiPerDiF method. In *International Conference on Manufacturing of Advanced Composites*, pages 1–8, Bristol, United Kingdom, 2015.

[18] Luiz Claudio Pardini and Luis Guilherme Borzani Manhani. Influence of the testing gage length on the strength, young's modulus and weibull modulus of carbon fibres and glass fibres. *Materials Research*, 5(4):411–420, oct 2002.

[19] Joël Henry and Soraia Pimenta. Semi-analytical simulation of aligned discontinuous composites. *Composites Science and Technology*, 144:1–15, 2017.

[20] Kimiyoshi Naito, Yoshihisa Tanaka, Jenn-Ming Yang, and Yutaka Kagawa. Tensile properties of ultrahigh strength PAN-based, ultrahigh modulus pitch-based and high ductility pitch-based carbon fibers. *Carbon*, 48:189–195, 2008.

[21] Cytec Industrial Materials. MTM 493 prepreg data sheet. Technical report, Cytec Industrial Materials, Derby, 2012.

[22] Sam A. Kaddour, Mike J. Hinton, Paul A. Smith, and Shuguang Li. Mechanical properties and details of composite laminates for the test cases used in the third world-wide failure exercise. *Journal of Composite Materials*, 47(20-21):2427–2442, sep 2013.

[23] Li-Min Zhou, Jang-Kyo Kim, and Yiu-Wing Mai. On the single fibre pull-out problem: effect of loading method. *Composites Science and Technology*, 45(2):153–160, jan 1992.

[24] Xi Zhang, Hong-Yuan Liu, Yiu-Wing Mai, and Xiao-Xue Diao. On steady-state fibre pull-out I The stress field. *Composites Science and Technology*, 59:2179–2189, 1999.

[25] MathWorks. bwlabel - MATLAB R2016b documentation. https://uk.mathworks.com/help/images/ref/bwlabel.html, 2016. [Online; accessed 23-March-2017].

[26] J Henry and S Pimenta. Modelling hybrid effects on the stiffness of aligned discontinuous composites with hybrid fibre-types. *Composites Science and Technology*, 152(1):1–15, 2017.

[27] Michael Wisnom. Mechanisms to create high performance pseudo-ductile composites. *IOP Conference Series: Materials Science and Engineering*, 139(1):1–9, jul 2016.

Appendices

Appendix A Calculation of the fracture toughness of fibres surrounding a cluster

The fracture toughness associated with a cluster of broken fibres within a composite material is dependent on the fracture toughness of the material surrounding the broken

cluster. For discontinuous composites [19] and *intermingled* hybrid discontinuous composites [10], the fracture toughness can be approximated as a constant value throughout the cross-section, because the arrangement of fibre types is homogeneous (or quasi-homogeneous).

However, this approximation of an average fracture toughness does not hold when applied to *intraply* hybrid discontinuous composites, as the fibre arrangement is no longer homogeneous. It is thus necessary to evaluate the fracture toughness associated with each cluster as the toughness of the material surrounding each individual cluster.

Figure 21 shows a detailed flowchart of how to evaluate the toughness of the surrounding material of a specific cluster. The process starts by identifying the kth cluster of broken fibres within the cross section, whose location is stored in a matrix $\boldsymbol{K}$. The matrix $\boldsymbol{K}$ is then translated around itself to the left, right, top, and bottom to identify all of the fibres surrounding the cluster (in this case a co-ordination number of four is used); the locations of the surrounding fibres are then stored in the matrix $\boldsymbol{S}$. The matrix of fibre types $\boldsymbol{T}$ and the matrix of surrounding fibres $\boldsymbol{S}$ are used to determine how many fibres of each fibre type surround the broken cluster; the translaminar fracture toughness of a single glass fibre composite and a single carbon fibre composite are calculated using the method described by Henry and Pimenta [19] (these values are shown in Table 1). Finally, the fracture toughness of the surrounding material $\boldsymbol{\mathcal{G}}_{\mathrm{I}}$ is calculated as the weighted average of each individual fibre type fracture toughness, based on the relative area occupied by each fibre type.

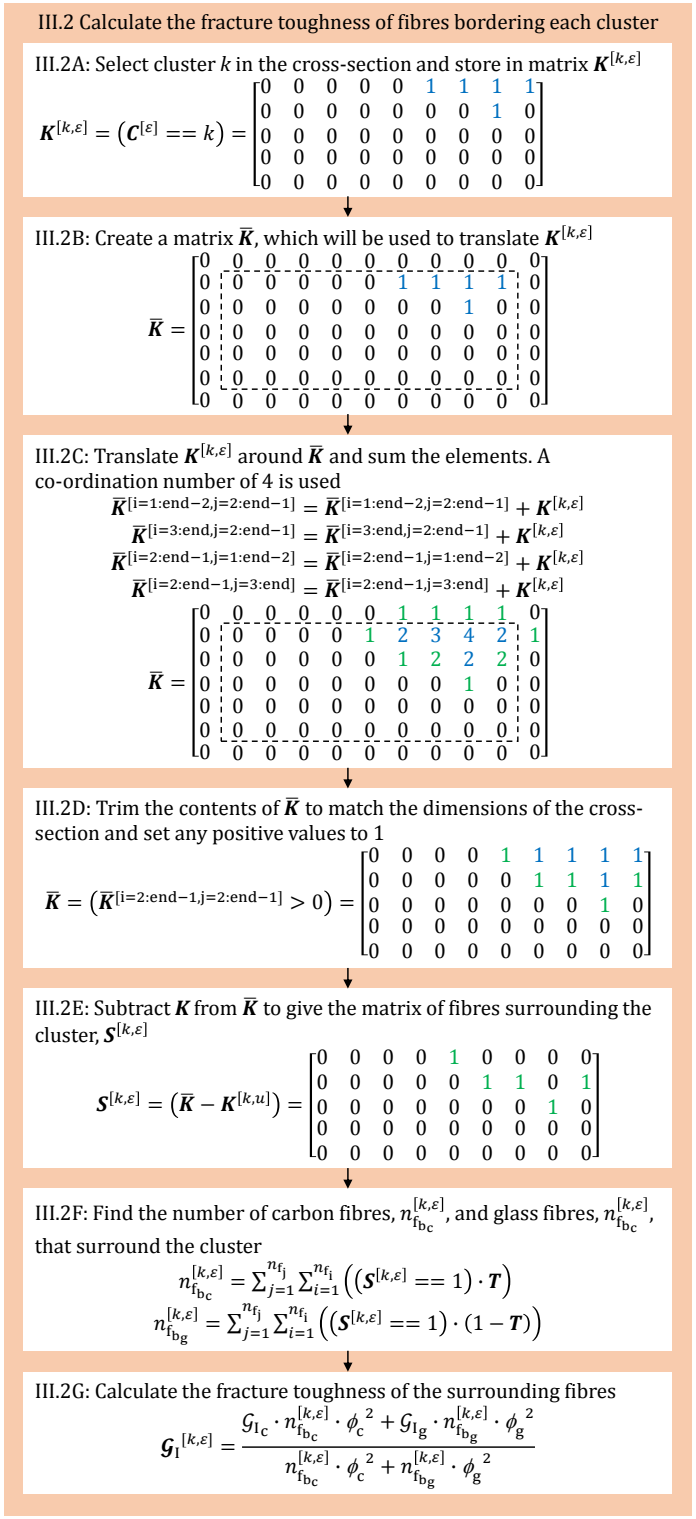

Figure 21: Flow chart to demonstrate how the fracture toughness of the material surrounding a cluster is calculated.